Structure and Dynamics of Tetrahalomethane Adsorption on (001) Surfaces of Graphite and α-Quartz

Gary M. Leuty[‡] and Mesfin Tsige*[,‡]

Department of Physics, Southern Illinois University Carbondale, Carbondale, Illinois 62901, United States

Received: July 13, 2010; Revised Manuscript Received: September 21, 2010

Molecular dynamics (MD) simulations were used to study the structural and dynamic properties of multilayer adsorption of each of three halomethanes, CF_4, CF_3Cl, and CF_3Br, adsorbed onto the (001) surface of either of two atomically flat but chemically and structurally different substrates (graphite and hydroxylated α-quartz) at temperatures ranging from 60 to 300 K. Analysis of the data shows a strong influence on the adsorption characteristics of these halomethane films due to the surface characteristics of the chosen substrate. In particular, the nature of the hydroxylation of α-quartz shows a striking ability to alter the affinity with which species adsorb onto its surface. This effect appears to be at least partly responsible for the differences in the orientation and packing of molecules in the first film layer as well as differences in the effect of temperature variation on phase behavior and dynamics.

Introduction

Organofluorine compounds comprise a very large class of organic molecules with wide-ranging properties, from surfactants to lubricants and nonstick coatings, numerous applications as refrigerants and in fire-suppression systems, and as plasma-etchants in microprocessor fabrication; even LCD technology owes some of its successes to fluorinated liquid crystals.[1] The factor most crucial to the desirable properties of organofluorine compounds is the carbon−fluorine bond, which, due to the high polarity induced by the large electronegativity of the fluorine atom, is the strongest bond known to organic chemistry. The addition of carbon−fluorine bonds to a single carbon in a compound serves to strengthen each bond at that carbon, thus highly substituted fluoroalkanes and related compounds have a unique stability that is responsible for many of their applications.[2]

However, despite extensive study of complex fluoroalkanes and the myriad applications discovered for fluoroalkane compounds, comparatively little effort is spent studying the basic behavior of simple fluoroalkane molecules, especially with regard to their interactions at adsorption surfaces. In the past, studies that have focused on adsorption of halomethanes, and specifically tetrahalomethanes, have largely centered on adsorption onto graphite.[3−8] While these studies have provided important insights into the adsorption behavior of specific halomethanes, we feel that there is a need to look critically at the differences between adsorption on a hydrophobic surface, such as the aforementioned graphite, and hydrophilic surfaces, including α-quartz, which is the second substrate of import in this study, for which we are aware of no extant studies on halomethane adsorption. Our motivation to examine adsorption on hydrophobic vs hydrophilic substrates stems from the idea that a number of fluorine-containing organic compounds show very different behavior on hydrophobic and hydrophilic substrates and thus suggests that studying these structures may provide important information on the behavior of organofluorine compounds in biological systems, where the difference between hydrophobic and hydrophilic surfaces has a profound effect on application.

We started our study with one of the simplest tetrahalomethanes, CF_4, tetrafluoromethane (or carbon tetrafluoride). As mentioned previously, the addition of carbon−fluorine bonds to a given carbon atom makes each existing carbon−fluorine bond even stronger than before; thus tetrafluoromethane becomes the most stable of the halomethanes because of its maximum number of carbon−fluorine bonds. While carbon−fluorine bonds are by nature highly polar, CF_4 is a nonpolar molecule, owing to four identical carbon−fluorine bonds positioned around the central carbon in a tetrahedral structure that cancels each bond's contribution to overall molecular polarity. As a result of this geometry and overall nonpolar nature, the CF_4 molecule is often thought of as being effectively spherical and can be viewed as behaving similarly to heavy rare gas molecules. Due to the unique nature of the carbon−fluorine bond, however, CF_4 molecules are observed to experience much different interactions compared with rare gas molecules, and the differences due to these interactions provide a very different phase behavior for CF_4 that provides a new set of possible applications, which has attracted some attention in recent years.[9]

To compare with the behavior of the nonpolar CF_4 molecule, however, we also decided to study the adsorption behavior of two very similar halomethanes that differ from CF_4 by only one atom—a change that carries profound implications with it. CF_3Cl (chlorotrifluoromethane) and CF_3Br (bromotrifluoromethane) have seen a number of applications, most notably as refrigerants (CF_3Cl, also known as Freon 13) and in fire-suppression systems (CF_3Br, also known as Halon 1301). Both molecules, due to replacing a carbon−fluorine bond with a bond of different polarity, obtain a net dipole moment (0.510 D for CF_3Cl, 0.651 D for CF_3Br[10]) and become aspherical; both these factors make these molecules simple to implement alongside CF_4 in our study yet offer important differences to contrast with the behavior of the nonpolar, spherical CF_4.

To study the adsorption of these compounds, we performed a series of molecular dynamics simulations of multilayer films

* To whom correspondence should be addressed: E-mail: mtsige@uakron.edu.

‡ Current address: Department of Polymer Science, The University of Akron, Akron, Ohio 44325-3909.

10.1021/jp1065049
Published on Web 10/20/2010

of CF_4, CF_3Cl, and CF_3Br on graphite and α-quartz (referred to as SiO_2 henceforth) over a range of temperatures from 60 to 300 K. Although most of our emphasis will rest on the structure of the layer closest to the surface (for reasons that will be explained in due order), we feel it is important to stress the multilayer context of our simulations as a crucial difference between this study and a number of previous studies that have focused on monolayer and bilayer coverages because of the difference between adsorption when few if any layers above the surface are present as opposed to adsorption in the presence of bulk adsorbate that may interact with the surface or with molecules closer to the surface.

We also feel it is important to stress that accurate modeling of these systems will likely require an all-atom approach, as was observed in our simulations. While all-atom simulations invariably increase the computational cost of simulations, the unique nature of organofluorine compounds, especially with respect to the fluorine atoms themselves, is expected to play a significant role in determining the phase behavior of adsorbed systems. Thus, we feel an all-atom approach is essential to gaining as much information on the structure and dynamics of adsorbed tetrahalomethane systems as we are capable of producing.

Methodology

Systems of interest in the simulations performed were composed of 1000 molecules of CF_4, CF_3Cl, or CF_3Br placed near the surface of one of two substrates: graphite or fully hydroxylated SiO_2 (silica group Q2 ($SiO_2(OH)_2$)). The graphite substrate was created with surface dimensions 54.12 Å × 51.13 Å × 20.10 Å (corresponding to seven graphene layers). The hydroxylated SiO_2 substrate was created with surface dimensions 54.05 Å × 51.06 Å × 18.14 Å, giving the two substrates very comparable surface areas and similar thicknesses. The thickness of each substrate was chosen so as to be larger than the cutoff distance of the van der Waals interaction (12 Å); thus interactions between the top and bottom surfaces of the substrate were considered negligible. The positions of the carbon atoms in the graphite substrate were frozen throughout each simulation, as has been done in recent simulations;[11−13] in contrast, the hydroxyl groups at the top surface of the SiO_2 substrate were allowed to vibrate about their points of attachment to the SiO_2 surface, and the positions of the remainder of the substrate atoms were frozen. Details of the generation of the hydroxylated SiO_2 substrate can be found in previous work.[14,15]

Intramolecular and intermolecular interactions between atoms were modeled using the optimized potentials for liquid simulations-all-atom (OPLS-AA) force field, developed by Watkins and Jorgensen.[16] In this force field, the total potential energy of the system is represented as the sum of four distinct potentials: nonbonding, bond-stretching, angle-bending and torsion, the latter of which is calculated as a four-body dihedral interaction of consecutively bonded atoms. The nonbonded potential was modeled as a combination of Lennard-Jones 12-6 potential and Coulomb potential,

$$u(r_{ij}) = 4\varepsilon_{ij}\left[\left(\frac{\sigma_{ij}}{r_{ij}}\right)^{12} - \left(\frac{\sigma_{ij}}{r_{ij}}\right)^{6}\right] + \frac{e^2 q_i q_j}{4\pi\varepsilon_0 \varepsilon r_{ij}} \qquad (1)$$

where r_{ij} is the interparticle separation, ε_{ij} is the depth of the potential well, σ_{ij} is the interparticle distance at which the potential is zero, q_i and q_j are the partial charges (in terms of the fundamental charge, e) assigned to atoms i and j, respectively, ε_0 is the vacuum permittivity, and ε is the dielectric constant. Lennard-Jones parameters for heteroatomic pairs are calculated using geometric mixing rules, as per the original OPLS formulation.[17] Values used for each of the parameters are available in Table 1. Note that silicon and oxygen atoms each have two different values for q, depending on whether they are bonded to surface hydrogen atoms, and carbon atoms have different values for all three parameters, depending on whether they are members of the graphite substrate or the adsorbate, as well as whether they are bonded solely to fluorine atoms or have one C−F bond replaced by either C−Cl or C−Br.

TABLE 1: OPLS-AA Force Field Parameters for Nonbonding Interaction

$u_{NB}(r_{ij}) = 4\varepsilon_{ij}[(\sigma_{ij}/r_{ij})^{12} - (\sigma_{ij}/r_{ij})^{6}] + e^2 q_i q_j/4\pi\varepsilon_0\varepsilon r_{ij}$

atom type	ε (kcal/mol)	σ (Å)	q (e)
C (substrate)	0.070	3.55	0.000
C (CF_4)	0.097	3.50	0.480
C (CF_3Cl)	0.066	3.50	0.422
C (CF_3Br)	0.066	3.50	0.380
F	0.053	2.95	−0.120
Cl	0.266	3.47	−0.062
Br	0.354	3.84	−0.020
Si_1	0.100	4.00	0.860
Si_2	0.100	4.00	0.960
O_1	0.170	3.00	−0.430
O_2	0.170	3.00	−0.683
H	0.000	0.00	0.000

TABLE 2: OPLS-AA Force Field Parameters for Bond-Stretching Interaction

$u_B(r_{ij}) = \kappa_{ij}^{bond}(r_{ij} - r_{ij}^0)^2$

bond type	κ_{ij}^{bond} (kcal/(mol Å^2))	r_{ij}^0 (Å^2)
C−F	367.0	1.332
C−Cl	245.0	1.781
C−Br	286.81	1.93

TABLE 3: OPLS-AA Force Field Parameters for Angle-Bending Interaction

$u_A(\theta_{ijk}) = \kappa_{ijk}^{ang}(\theta_{ijk} - \theta_{ijk}^0)^2$

bond type	κ_{ijk}^{ang} (kcal/(mol rad^2))	θ_{ijk}^0 (deg)
F−C−F	77.00	109.1
F−C−Cl	100.0	109.5
F−C−Br	100.0	109.5

The bond- and angle-bending terms were both modeled as harmonic potentials,

$$u_B(r_{ij}) = \kappa_{ij}^{bond}(r_{ij} - r_{ij}^0)^2 \qquad (2)$$

$$u_A(\theta_{ijk}) = \kappa_{ijk}^{ang}(\theta_{ijk} - \theta_{ijk}^0)^2 \qquad (3)$$

where r_{ij} is the distance between bonded atoms i and j, θ_{ijk} is the angle created by consecutively bonded atoms i, j, and k, and κ_{ij}^{bond}, r_{ij}^0, κ_{ijk}^{ang}, and θ_{ijk}^0 are respectively the force constant of the bond-stretching potential, the equilibrium bond length, the force constant of the angle-bending potential, and the equilibrium angle value. Values for these constants are presented in Tables 2 and 3.

Owing to their simple geometry, the adsorbate molecules themselves were not expected to require the addition of a torsional potential. However, because the hydroxyl groups of the hydroxylated SiO_2 substrate were allowed to vibrate, torsional contributions were added for these groups.

Each system underwent an initial bulk equilibration in the isothermal−isobaric (*NPT*) ensemble, with periodic boundary conditions extending in all directions, at temperatures above the bulk melting temperature of each system for a period of 4 ns, with bulk equilibration occurring well within this interval. For adsorption simulations, the equilibrated bulk system was initially placed 5 Å above the substrate surface, to allow the widest possible latitude in selection of adsorption sites. This vacuum separation was within the range of the van der Waals interaction, and as such, the bulk liquid was able to adsorb en masse.

All adsorption simulations were performed using the LAMMPS molecular dynamics package[18] and were run in the canonical (*NVT*) ensemble, using the velocity-Verlet algorithm to integrate the equations of motion of the particles with a 1 fs time step. A Nose−Hoover thermostat was employed to regulate the system temperature in each simulation, and simulations in each class were run for a variety of temperatures in the range from 60 to 300 K, largely in increments of 10 K. The van der Waals interaction was given a cutoff distance of 12 Å; tests were also performed using a larger cutoff (15 Å) and were shown to produce no observable changes in the outcomes of the simulations. Long-range Coulombic interactions were calculated using the particle−particle/particle−mesh (PPPM) algorithm.[19] Periodicity was again extended in all directions; however, to avoid effects from images due to periodicity in the direction normal to the surface, the simulation box was extended in the *z*-direction to simulate a large vacuum space above the adsorption surface. Simulations were performed in two phases: an equilibration phase lasting ∼4 ns (∼4 000 000 time steps), followed by production runs lasting 1.5 ns (1 500 000 time steps), with atom positions recorded every 1 ps (1000 time steps) for analysis.

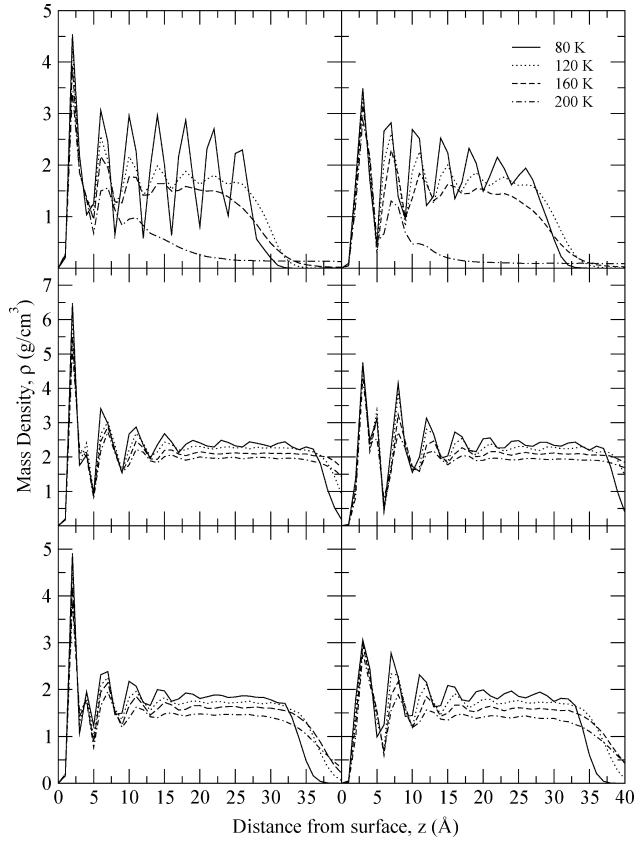

Figure 1. All-atom mass density as a function of distance from the surface for several temperatures of simulations of CF_4 (top row), CF_3Br (middle row), and CF_3Cl (bottom row): left column, molecules adsorbed on graphite; right column, hydroxylated SiO_2.

Results and Discussion

Structural Analysis. Figure 1 shows the average density profiles of the various films as a function of *z*, the distance normal to the surface of the substrate. Profiles were obtained by partitioning the simulation cell into bins along the *z*-direction and calculating the average density within each bin with respect to each atom and its position.

The most immediate conclusion drawn from a look at Figure 1 is the presence of layering, noted by pronounced density oscillations, that appears to persist to a depth of at least 15−20 Å in all cases, and even further in cases of adsorption at low temperatures (to ∼20−25 Å for temperatures 120 K and below). At high temperatures, the densities quickly begin to approach their respective bulk values (approximately 1.6 g/cm^3 for liquid CF_4 (obtained from previous simulation), 1.78 g/cm^3 for liquid CF_3Cl at 120 K, and 2.12 g/cm^3 for liquid CF_3Br at 120 K)[20] and the number of oscillations pointing to distinct layers begins to decrease dramatically. The exact number of layers discernible varies increasingly as we reach the high end of our simulation temperature range, and in the case of CF_4, we see that as we increase the temperature to approximately 200 K and above, molecules begin to evaporate and show the much lower density noted in Figure 1.

At low and intermediate temperatures, generally five or more layers are noted in all cases, with CF_4 films and polar-molecule films on hydroxylated SiO_2 showing up to seven distinct layers. This result would appear to contradict a previous experimental study[7] of CF_4 adsorbed on graphite in which the layering of adsorbed films is limited to at most two layers below 71 K, with subsequent layers appearing individually as temperature is increased. One may be able to resolve this disparity by noting that the experimental study was based on vapor-phase adsorption of the CF_4 molecules, whereas in our study, the simulation centers on adsorption of liquid molecules (in all cases) onto their respective substrates after having been released into a small vacuum space originally placed between the adsorbate and substrate. This approach allows the liquid to equilibrate as a bulk system next to a substrate throughout the simulation and presents a fundamentally different mechanism for adsorption versus the vapor-based deposition technique used experimentally. It should be noted that in the cases of CF_3Cl and CF_3Br adsorption on either substrate, or CF_4 adsorbed on hydroxylated SiO_2, we are currently unaware of experimental or theoretical trials that study multilayer adsorption, and thus we feel this study presents a view on multilayer adsorption that, to our knowledge, does not currently exist.

Examining the oscillations in average mass density of each film, we see the first signs of structural differences as a result of changing the substrate type. In Figure 1, we see that the first layer of CF_4 adsorbed on graphite has a peak density that appears higher than that of the first layer on hydroxylated SiO_2 at 80 K, and similarly for CF_3Cl and CF_3Br, and this can offer information on the expectation of ordering within the layer. As temperature increases, the peak first-layer density of all three films adsorbed on graphite remains higher, suggesting that there may be a difference in packing in the first layers caused by the choice of substrate type and independent of temperature resulting in a lower first-layer density of molecules adsorbed on hydroxylated SiO_2 compared to graphite. When we move to the second layer, this trend largely reverses itself, with peak density being higher for the polar films on hydroxylated SiO_2, and nearly

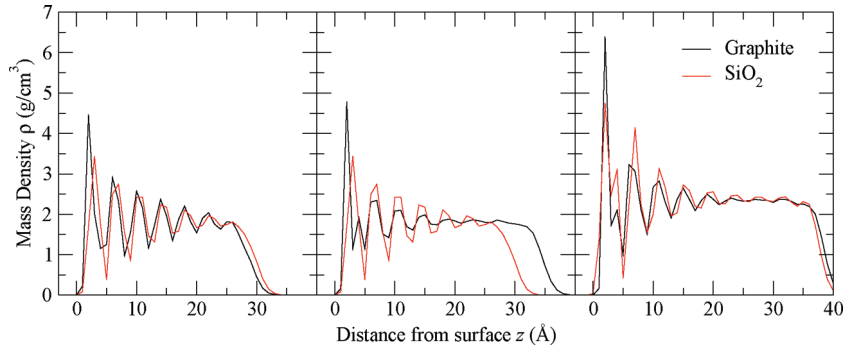

Figure 2. Mass density vs distance from the surface at 90 K for simulations of CF_4 (left), CF_3Cl (middle), and CF_3Br (right).

equal for CF_4, which may suggest that the effect that made films close to the graphite surface more dense is diminished or not present at all. At 200 K, polar films show only weak oscillations to the third and fourth layers; however, the observed density beyond these layers at this temperature is still well within the expected density of the bulk liquid, whereas CF_4 films largely decay to vapor-phase densities beyond the second layer (having traversed the bulk boiling point at 145.1 K).[21] Visualizations of the systems show that only the first layer above the substrate survives nearly intact as we increase the temperature even moderately (at ∼150 K, even the second layer begins to break down), and thus the focus of our study becomes the first layer, in the context of a multilayer film, which provides the only layer system persistent enough to gather consistent data on adsorption.

From the density oscillations, we can infer general characteristics of the layers as well as the dependence of packing density as a function of temperature. From this, we may begin to examine possible explanations for differences in packing density based on possible structural differences between adsorbate molecules. For films on both graphite and hydroxylated SiO_2, the peak density of corresponding layers is seen to decrease with increasing temperature, as one may expect; however, the peak densities themselves do not suggest exactly how closely packed the molecules are. For this, we used the density data we collected to calculate the average number of molecules in the layers per unit surface area of the substrate (henceforth referred to as MPA). In the case of CF_4, these data appear to reflect the trend seen in Figure 1. From the peak density seen in the figure, we suggest that the first-layer density of CF_4 on the graphite substrate is larger than it is for CF_4 on hydroxylated SiO_2, reflecting denser packing of molecules. Our calculations bear this out: at all temperatures, the CF_4 film adsorbed on graphite shows MPA between 4% and 15% greater than the same films on hydroxylated SiO_2. Greater disparity between the substrate types is seen over the whole temperature range shown in Figure 1, as we have calculated an MPA decrease of roughly 12% for CF_4 on graphite, compared to only 5% for CF_4 on hydroxylated SiO_2 over the 120 K range pictured in the figure.

Polar molecules, on the other hand, show very different behavior. Whereas the thicknesses of the first layer for films of CF_4 were similar for either substrate, there appears to be a slight disparity in first-layer thickness for polar films, with the films on hydroxylated SiO_2 appearing slightly thicker than the films on graphite. Thus, while the peak densities of polar films on graphite are demonstrably larger (from Figure 1), the average number of adsorbed molecules per unit area is quite different. At each temperature studied, films of CF_3Cl on hydroxylated SiO_2 were at least 10% more densely packed than the same films on graphite, and the difference was even more pronounced for CF_3Br films, where the calculation of MPA shows films on hydroxylated SiO_2 to be 35% more densely packed, or more, than their counterparts on graphite. Polar films did show behavior similar to that of nonpolar CF_4 films, however, in that the effect of temperature appears muted for films on hydroxylated SiO_2, from both the figure and calculation, compared to the same films on graphite. While polar films on graphite showed a roughly 10% decrease in the number of molecules on the surface per unit area, the same films on hydroxylated SiO_2 tended to show decreases under 5%. From this, we infer that the two substrates have very different affinities for the halomethanes studied in our simulations, as it would appear molecules adsorbed onto the hydroxylated SiO_2 surface exhibit some resistance to temperature-based desorption.

In Figure 2, we can see by comparison of each case across substrate type that while the choice of substrate has minimal effect on the depth to which ordering occurs, it does appear to influence the density of each layer as one gets further from the surface. The peak density of the first adsorbed layer on graphite represents increases of 30−40% for films of CF_4, CF_3Br, and CF_3Cl on SiO_2. Densities at the second layer and beyond are very comparable in the case of CF_4 films, while CF_3Cl and CF_3Br films show a slightly higher density for films adsorbed on SiO_2. From Figure 2, we also note a slight shift in the positions of the peak first-layer densities in all three cases; the maximum density of films on SiO_2 is shifted slightly away from the surface, in comparison with the graphite substrate, which suggests a shift in the positions of the atoms in each case relative to the normal to the surface for both CF_4 and CF_3Cl; however, the position of the peak of the density of the first layer of CF_3Br appears to be unaffected by substrate choice.

The question of why the polar molecules appear to pack more densely on hydroxylated SiO_2, while CF_4 appears to pack more densely on graphite, can perhaps be suggested by examining the shapes of the molecules themselves. CF_4, having four equal C−F bonds arranged in tetrahedral geometry, comes closest to approximating a spherical molecule. The substitution of one of the fluorine atoms in CF_4, however, results not only in the appearance of a net dipole moment but also in a large shift in molecular shape, as both the chlorine atom and the bromine atom are significantly larger than the fluorine atoms they replace, This leads to a net asphericity of the polar molecules, which may have implications for packing arrangements, depending on how the molecules array themselves within the layers.

In the case of the polar molecules CF_3Br and CF_3Cl, examining the general orientation of the molecules can readily be done by examining the C−Cl and C−Br bonds. In each case, we calculated the angle between the C−Cl or C−Br bonds and the z-axis (surface normal) and collected the data into the distribution seen in Figure 3.

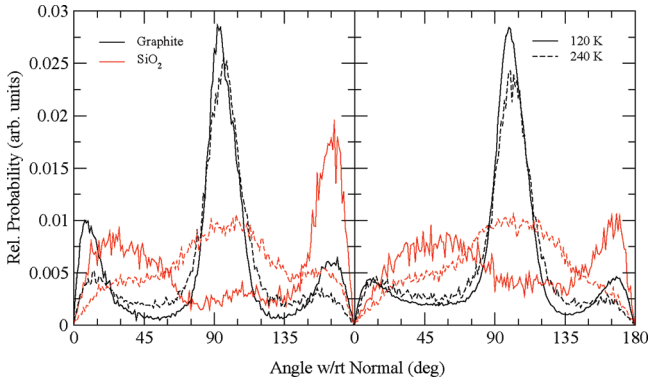

Figure 3. Probability distribution for the angle between the C−Cl of CF_3Cl or C−Br bond of CF_3Br and the surface normal at two different temperatures: left, CF_3Br; right, CF_3Cl.

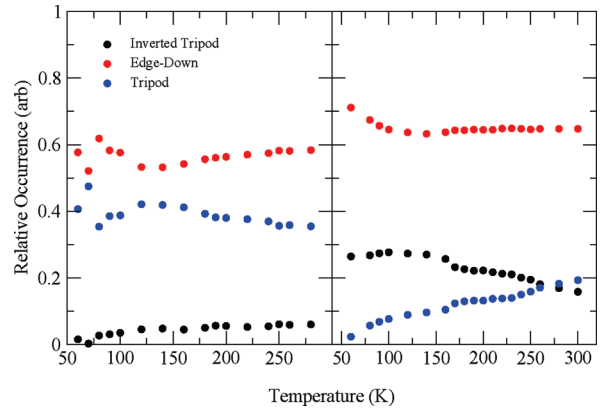

Figure 4. Percentage of molecules in a given configuration as a function of simulation temperature: left, CF_4 on graphite; right, CF_4 on SiO_2.

In both cases, we see that the molecules adsorbed on graphite have a definite preferred arrangement, with the C−Cl or C−Br bond oriented just past the horizontal, pointing toward the surface, slightly more so in the case of CF_3Cl. Subsequent analysis suggests that these bonds, together with two of the C−F bonds, form an F_2Cl "tripod" that rests on the substrate surface. In the case of CF_3Cl, this result is supported by an X-ray diffraction study that suggests the F_2Cl tripod arrangement is expected to be indicative of a stable phase.[22] The same study also makes mention of an arrangement involving molecules resting on the F_3 tripod (this is expected for the commensurate phase, which is expected to behave much like CF_4). While we note the presence of the F_3 tripod arrangement as well (corresponding to a C−Cl or C−Br orientation of ∼0°), it does not appear to occur in the same manner as the commensurate 2 × 2 solid phase; this may be a point for further analysis. The F_2Cl and F_2Br tripod arrangements, along with the much higher density of chlorine and bromine compared to carbon and fluorine, provides a much greater mass closer to the substrate surface, which is noted in the first large peak in density in each case in Figure 2. In both of the polar cases, a noticeable secondary peak is seen just after the main first-layer density peak. For CF_3Br, this is due to the presence of the notable population of molecules in which the F_3 tripod rests on the surface, and the C−Br bond points away from the surface (corresponding to the smaller peak at low angles in Figure 3); due to the large mass of the bromine atom, this corresponds to a sizable density located near the boundary of the first layer. In the case of CF_3Cl, the opposite appears to be true: at low temperatures, a lesser number of molecules are oriented as inverted tripods, with C−Cl bond pointing toward the surface. This leaves the more massive F_3 groups toward the boundary of the first layer and produces a diminished secondary density peak near the end of the first layer.

For polar molecules on SiO_2, the situation is much different. In both cases, we see in Figure 3 that one of two orientations is favored: either the C−Cl or C−Br bond is tilted between 0 and 90° from the surface normal, distributed widely over this region, or the C−Cl or C−Br bonds point toward the surface, deflected slightly from vertical. In CF_3Br, the number tilted from the negative z-direction is larger than those tilted more randomly from the positive z-direction; thus the unequal distribution of mass and angular orientation again gives a two-peak result for the first-layer density. CF_3Cl, however, shows nearly equal numbers deflected from the negative z-direction as are more widely deflected from the positive z-direction - this, and the distribution of mass in the CF_3Cl molecule, appear to combine to give a fairly uniform first-layer density that is shifted toward the center of the first layer, as opposed to the two-peak density seen in the previous cases. As we increase the simulation temperature, we see that the orientations of the polar molecules on SiO_2 become very similar in character, as the C−Cl and C−Br bonds in both cases prefer an orientation slightly past parallel to the surface, as was noted for the same molecules adsorbed on graphite.

The orientation of CF_4 molecules is less readily apparent. The symmetry of the CF_4 molecule makes it nearly spherical, which rules out the use of a lone bond to categorize differences in orientation. Instead, we looked at the relative position (in the z-direction) of the fluorine atoms relative to the carbon atom to see how the fluorines arranged around the center of the molecule. The result is a calculation that gives the relative number of CF_4 molecules in the tripod configuration, an edge-down configuration in which two fluorine atoms rest near the surface and the top seems to pivot on this edge, or the inverted tripod configuration. The data are shown in Figure 4.

The distribution of the orientation of CF_4 on graphite shows a large combined population of tripod and edge-down molecules, which places more of the more massive fluorine atoms closer to the surface; the edge-down configuration might be expected to contribute equally to the first density peak over the entire first layer, but the tripod population is sufficiently large to put a sizable number of F_3 groups at the surface. The opposite is true for CF_4 molecules on SiO_2, for which low temperatures show a majority of edge-down molecules seconded by inverted tripod molecules, which places the more substantial amount of mass further from the surface and shifts the peak density in the first layer further away and helps to explain the shift in the first-layer peak density. A separate result is seen in Figure 4 in that while the distribution of CF_4 orientations on graphite appears nearly constant as temperature is increased, there appears to be a shift in populations in the case of CF_4 on SiO_2, as at higher temperatures, tripod-oriented molecules begin to overtake inverted-tripod molecules in terms of population. This suggests a possible inversion of molecular orientation as a function of temperature.

To determine the presence of other evidence of any sort of transition, we looked at other measures of structural order on the first layer. The in-plane radial distribution function, $g(r)$,[4] is defined as

$$g(r) = \frac{A}{N^2}\left\langle \sum_i \sum_{j \neq i} \frac{H(r_{ij} - (r - \Delta r/2))H((r + \Delta r/2) - r_{ij})}{2\pi r \Delta r} \right\rangle \quad (4)$$

where H represents the unit step function, and the distance between molecules is divided into bins of width Δr. The radial distribution function gives a measure of the average number of molecules within a distance r of an arbitrary particle, with the first and subsequent peaks representing nearest neighbors, second-nearest neighbors, and so on. The radial distribution function is one method quantifying positional correlations between molecules within a given layer, providing information on correlations within the layer, which may detail any phase transitions present. It is also a useful quantity due to its relation to the static structure factor, $S(q)$, which can be determined from diffraction analysis.[23,24] In the present study, the carbon atoms of each molecule were used as reference points for the locations of the molecules; thus the $g(r)$ calculations shown more accurately reflect the carbon−carbon radial distribution, $g_{CC}(r)$, and references to $g(r)$ herein refer to $g_{CC}(r)$ unless specifically noted otherwise. Although the molecules are not precisely within the same plane parallel to the substrate surface, the spacing between layers was noted as being commensurate with the size of a single molecule, and thus the molecules can be regarded as existing within a single plane. Figure 5 shows plots of $g(r)$ for representative temperatures of 80, 140, 200, and 260 K; data were collected for a number of simulations ranging from 60 to 300 K.

From Figure 5, it is immediately clear that the choice of substrate has a major effect on the presence of long-range positional order. This is especially true in the cases of the polar molecules CF_3Br and CF_3Cl on graphite, which show small first-neighbor amplitudes that decrease to unity (i.e., no positional order) within 15−20 Å and decrease steadily with increased temperature. In these polar-molecule films on graphite, the temperature dependence of the peak amplitudes is difficult to discern but most noticeable for the small secondary peak that occurs after the peak of the first nearest neighbor. This secondary peak is likely due to the differences in orientation of the C−Cl or C−Br bond within the layer plane at low temperatures. The radial distribution seen in these cases does bear some resemblance to particles in a rhombic lattice, although the rapid decay of peaks makes a conclusive determination difficult. The secondary peaks diminish and combine with the main peak as temperature increases, implying variation in temperature serves to randomize the C−Cl or C−Br orientations and further affect the nature of the positional order seen. Oscillation decays suggest that the first layers of these films may be in a liquid phase even at low temperatures, and indeed, there is evidence of a significant melting-point depression in submonolayer films of both CF_3Cl and CF_3Br on graphite[25] with respect to the bulk melting temperature of 92 K.[26] However, addition of molecules to the submonolayer films to form a compressed monolayer is shown in the same study to cause an increase in melting temperature with respect to the submonolayer, while still being lower than the bulk melting temperature. We are unaware of any study detailing whether melting temperature at the first layer should continue to increase in the multilayer case, or whether the addition of multiple layers above the first allows a relaxation of the first layer and reverses this trend.

Additionally, there is a notable shift in the position of nearest neighbors away from their low-temperature values as we increase the simulation temperature, both in the case of polar films and in some cases of CF_4 films. The effect only occurs

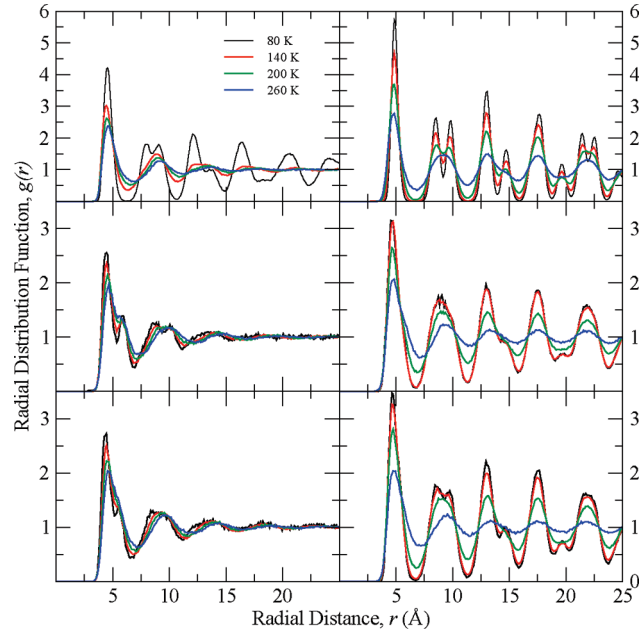

Figure 5. Plot of radial distribution function, $g(r)$, for CF_4 (top row), CF_3Br (middle), and CF_3Cl (bottom) on graphite (left column) and SiO_2 (right column) substrates.

after the radial distribution function suggests that positional order has decreased significantly, in general, an indication of a transition to the liquid phase. However, the change in molecular shape due to the asphericity introduced by the chlorine or bromine atoms in turn makes the orientations of these molecules on the surface an important consideration. Geometrical frustration (significant deviation due to inability to form regular packing structures) of the perfect hexagonal arrangement (seen in the case of the more spherical CF_4), due to irregular packing as a result of this asphericity, may explain the relatively featureless in-plane radial distribution functions seen. This suggests that the in-plane radial distribution function alone may not be enough to determine whether the layer has transitioned to the liquid phase, as $g(r)$ would indicate, or whether it is in a disordered crystalline solid with low long-range positional order.

In polar films on the hydroxylated SiO_2 substrate, as well as nonpolar CF_4 films on both substrates, the situation is quite different. In the case of CF_4 on graphite, Figure 5 shows the first layer of the film possesses definite structure at 80 K; the presence of a sharp first neighbor peak and subsequent peaks differing markedly from unity suggest the film is crystalline at this temperature. Previous investigations[27] have shown that the first layer of CF_4 films on graphite appear to be in the crystalline phase from 60 to 100 K, at which point the first layer is seen to still possess a relatively high degree of order but may be in the process of a transition to the liquid phase. Indeed, as seen in Figure 5, CF_4 films on graphite at 140 K and higher possess a much decreased first peak amplitude (from 80 to 140 K, the first peak amplitude decreases 28%) and rapidly decreasing nearest neighbor peaks thereafter, which is highly indicative of a liquid or liquid-like phase. CF_4 films on the hydroxylated SiO_2 surface, on the other hand, maintain a high degree of positional order at much higher temperatures relative to the same films on graphite. In Figure 5, although the peak amplitude of $g(r)$ is shown to decrease steadily as temperature increases, the first layer of the CF_4 films on SiO_2 maintain a regular oscillatory profile for cases below 260 K; at 260 K, although several of the peaks seen at lower temperatures have converged into broad

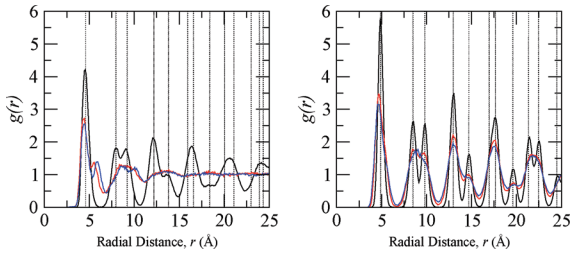

Figure 6. Radial distribution function plots for CF_4 (black), CF_3Cl (red), and CF_3Br (blue) at 80 K on graphite (left) and hydroxylated SiO_2 (right). Dashed lines represent positions of peaks for perfect hexagonal packing.

single peaks, the oscillations seen in the $g(r)$ profile indicate a relatively high degree of positional order remains.

There is also a large difference seen between $g(r)$ for the first layer of polar films on graphite and hydroxylated SiO_2. Similarly in character to the nonpolar case, the first layers of CF_3Cl and CF_3Br show the presence of distinct peaks varying significantly from unity, signifying defined neighbor positions and a high degree of order for cases below 260 K. The positions of nearest neighbor peaks in these cases are similar to those for CF_4, suggesting similar overall structures, but the individual peaks seen at the second-nearest neighbor position and further in the case of CF_4 on hydroxylated SiO_2 are not present in the polar cases. In these cases, the peaks seem to have combined, suggesting that although the two cases enjoy a similar structure, there is variation in the positions of the carbon atoms in the polar films that is not seen in the nonpolar films. This is likely due at least in part to the asphericity of the polar molecules, which lends itself to differences in molecular orientation that will broaden the range of possible carbon locations, while keeping the molecules in the same general positional configuration.

Having calculated the radial distribution function for each case, it is important to determine what the information presented in the radial distribution function says about the overall structure of film layers near the substrate surfaces. Previous study[6] has shown that in CF_4 films adsorbed onto graphite substrates, layers near the substrate surface prefer to adsorb in phases whose specific character shows a complex dependence on coverage and temperature but appears to prefer hexagonal geometry. Other studies have suggested similar packing arrangements (hexagonal or triangular) may be preferred in the case of the polar adsorbates.[25,28] With this in mind, we also calculated $g(r)$ for ideal hexagonal layers with the same nearest-neighbor distance, to use as a comparison to determine how the position of peaks in the radial distribution function corresponds to specific packing behavior. The results, compared to low-temperature $g(r)$ for the systems investigated, are shown in Figure 6. From this, we see that the first layer of CF_4 on graphite is in good agreement with the ideal structure to the fifth nearest neighbor, at which point the structure begins to deviate and further long-term positional order becomes less definite. In the case of polar adsorbates, however, the presence of a secondary peak just beyond the first is something that is not seen in the case of hexagonal packing but can be seen in the case of a rhombic lattice, as previously mentioned. Beyond these first two peaks, $g(r)$ for polar films become even less like the ideal hexagonal arrangement. Comparing to the higher temperature cases seen in Figure 5, the structure of the first layer of CF_4 on graphite shows long-range positional order at temperatures below roughly 100 K, at which point a transition appears to take place, and much of the positional order is lost.

In the case of each of the films on hydroxylated SiO_2, however, we see that the position of peaks in $g(r)$ corresponds

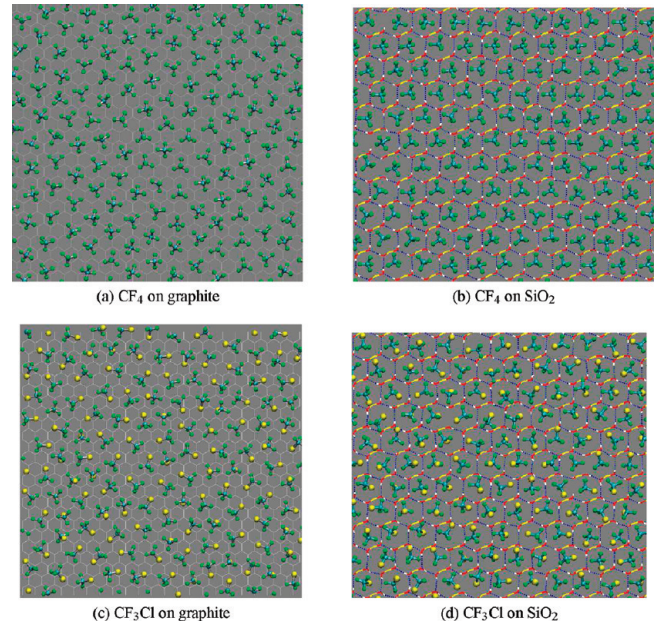

Figure 7. Snapshots of polar and nonpolar systems at 60 K. The CF_3Br system is similar in character to CF_3Cl. Only the uppermost part of each substrate surface is shown. Atom coloration: cyan, carbon; green, fluorine; yellow, chlorine (in adsorbate atoms) or silicon (in substrate); red, oxygen; white, hydrogen. Blue dashed lines in SiO_2 cases are used as a guide to the eye regarding hydrogen bonding at the surface. Gray lines in the graphite cases represent the structure of the graphite substrate.

very closely with the ideal hexagonal layer, demonstrably so in the case of CF_4. Coupled with the sharpness of the individual peaks, it becomes evident that first-layer CF_4 on hydroxylated SiO_2 is in a very stable hexagonal phase, which persists to much higher temperatures. In the case of polar films, the sharpness of the double-second peak is less definite (or essentially absent, as is the case with CF_3Br), suggesting possible deviation from the ideal hexagonal arrangement, but the agreement with subsequent peak locations enforces the idea that the polar films are packed in a highly ordered hexagonal lattice. This result is all the more interesting because, during the course of our investigations, we were aware of no a priori reason that the first layers of films adsorbed on SiO_2 should behave in this manner.

Figure 7 shows several snapshots taken with VMD[29] of the first layer of polar and nonpolar films at 60 K, along with the uppermost surface atoms of the substrate, using the low-temperature system to illustrate the structure of the crystalline phase. The structures displayed in Figure 7 appear to agree with the results from our $g(r)$ calculations: CF_4 presents as having local positional order in a hexagonal arrangement. Beginning at 120 K, a transition to the liquid phase appears to be taking hold, and positional order decreases sharply. The polar films adsorbed on graphite behave quite similarly to one another, as evidenced by $g(r)$ calculation as well as visualization (for this reason, CF_3Br is not included in Figure 7). In these cases, adsorbed films on graphite show little discernible order in the first layer; overall, $g(r)$ for these cases bears a small resemblance to the hexagonal structure of the first layer of CF_4 on graphite; however, as previously mentioned, polar molecules in the first layer on graphite prefer an orientation that places the carbon and chlorine or bromine atoms very nearly in the same plane.

In contrast, the visualizations of the first layers on the hydroxylated SiO_2 substrate offer a great deal of insight into the reasoning behind their orderly structure. Yang and Wang[30]

showed from ab initio calculations that on a clean (0001) surface of hydroxylated α-quartz (of a type identical to the SiO_2 substrate utilized in our simulations), hydrogen bonding between neighboring hydroxyl groups creates a network of alternating strong and weak hydrogen bonds that produces a zigzag pattern on the surface, much as the zigzag pattern of hydroxyl groups seen in Figure 7b,d. Including the hydrogen bonds in these visualizations, we see that the hydrogen bonding of the hydroxyl groups on the surface serves to create hexagonal "cells" along the hydroxylated SiO_2 surface, and that in both the polar and nonpolar cases, the adsorbed molecules prefer to remain inside these cells, crossing neither the silanol groups on the surface nor the hydrogen bonds between hydroxyl groups. Confinement to these hexagonal cells provides the greater degree of positional order seen in the $g(r)$ calculations, both in the CF_4 film and in CF_3Cl and CF_3Br; from the visualizations, it can be inferred that the sharpness of the $g(r)$ peaks seen in the case of CF_4 on hydroxylated SiO_2 is due to CF_4 molecules being nearly centered within the hexagonal cells. Variability in the orientation of the C−Cl or C−Br bonds in the polar cases gives rise to less definite positions within the cells, which causes the joining and broadening of the peaks seen in the radial distribution function. Still, the overall structure is presented as hexagonal due to the lateral confinement. Previously, we have studied the effect on packing of forcing the hydroxyl groups at the surface of the SiO_2 substrate to remain perfectly rigid and upright. In the case of CF_4, the result seen[27] suggests that it is indeed the presence of the hydroxyl groups that confines the adsorbed fluoromethanes to specific regions; in the cited case, the CF_4 molecules are forced to lie in channels created by lines of hydroxyl groups, with few or no CF_4 molecules approaching or crossing the hydroxyl "barriers." The $g(r)$ in this case suggests a nonhexagonal packing arrangement, due to variability of the intermolecular spacing within the channels. The result for CF_4 in this case is directly applicable to the polar adsorbates as well—the added asphericity of the polar molecules causes them to lie in channels with the polar axis along the channel, but with no appreciable preference for direction.

While the radial distribution function points toward the type of first-layer structure in the adsorbed films, it can be difficult to derive adequately the phase of the adsorbed layer from the radial distribution function alone. Liquid systems previously studied[31,32] show radial distribution functions with few defined peaks, a low first peak, and second and third peaks that do not split. This certainly agrees with the $g(r)$ calculations for the polar films on graphite and high-temperature (~260 K) systems, but for systems such as the polar films on silica, low-temperature cases show defined peaks, but ones that do not always split. The extent of the oscillations would seem to suggest these are indicative of the crystalline phase but make it difficult to pinpoint the melting transition with respect to temperature.

We also calculated the in-plane orientational order parameter, Φ_6,

$$\Phi_6 = \langle |\Psi_6(r)| \rangle = \left\langle \left| \frac{1}{N_b} \sum_{k=1}^{N_b} e^{i6\theta_k} \right| \right\rangle \quad (5)$$

Here, θ_k is defined as the angle between the vector joining the positions of the carbon atoms of neighboring molecules and an arbitrary axis; the sum runs over all neighbor pairs for a given molecule, and then the average is computed for all molecules in the first layer. Molecules defined as being a "neighbor pair" are those molecules whose carbon atoms are within the first minimum distance of the radial distribution function. When the molecules are packed in a perfect two-dimensional hexagonal crystalline structure, Φ_6 is expected to equal 1, while a disordered (liquid) phase is expected to give $\Phi_6 = 0$.[33,34]

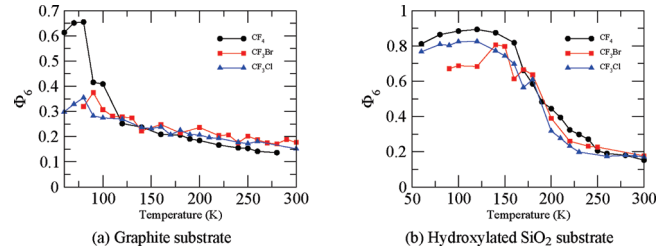

Figure 8. Average bond orientational order parameter for first adsorbed layers on graphite and SiO_2 substrates.

CF_3Cl and CF_3Br on graphite show only moderate orientational order at low temperatures and a linear decrease in average orientational order with increasing temperature, which is in line with our $g(r)$ data showing low positional order at all temperatures studied (see Figure 8a). Together, it is implied that the first layers of these films are either in the liquid phase or in a configuration significantly deviated from an ideal hexagonal arrangement at low temperatures, and that the structures only become less hexagonally ordered as the system temperature increases. CF_4 on graphite, on the other hand, possesses notably more orientational order at lower temperatures, with a pronounced transition to low orientational order beginning at 100 K and largely complete by 140 K; similarly, a decrease in positional order from $g(r)$ calculations is seen in Figure 5, with the hexagonal arrangement of the crystalline phase at 80 K replaced by a liquid-like phase by 140 K. Here, the rapid decrease of both orientational and positional order within this range suggests that the melting transition for the first layer of CF_4 on graphite takes place between 100 and 140 K, above the bulk melting point of CF_4, 89.5 K[7].

As previously mentioned, Figure 5 shows that positional order of the first layers of the same films on the hydroxylated SiO_2 surface remain high at 200 K, which is well above the bulk boiling points of CF_4 and CF_3Cl and not far below the bulk boiling point of CF_3Br. Looking at Φ_6 in Figure 8b, we get a result that fits this expectation and also provides an unexpected result. In the figure, we see that the orientational order of all three films remains quite high for temperatures below 150 to 160 K and begins to decrease slowly, reaching minimum values after a further increase of roughly 100 K. Comparing to our $g(r)$ calculations for positional order, we see CF_3Cl and CF_3Br systems are beginning to lose positional order around 200 K and have become liquid or liquid-like by 260 K, which correlates well with the average bond orientational order. Of particular note is the region of steepest decline in the orientational order parameter of the first layer on hydroxylated SiO_2. While the orientational order is not equivalent in magnitude at low temperatures, the onset of the order−disorder transition is at the same temperature, regardless of adsorbate type, and values of the order parameter both during and after the transition are quite comparable.

Dynamics. ***First-Layer Residence Time.*** So far, the choice of substrate shows a demonstrable effect on lateral positioning and orientation of the first layers of our adsorbed films. This offers one characterization of the effect of substrate choice on the adsorption of simple fluorocarbons. To look at how the choice of substrate affects how well molecules remain adsorbed on the substrate surface, our analysis shifted to dynamic considerations, including the residence time of molecules on

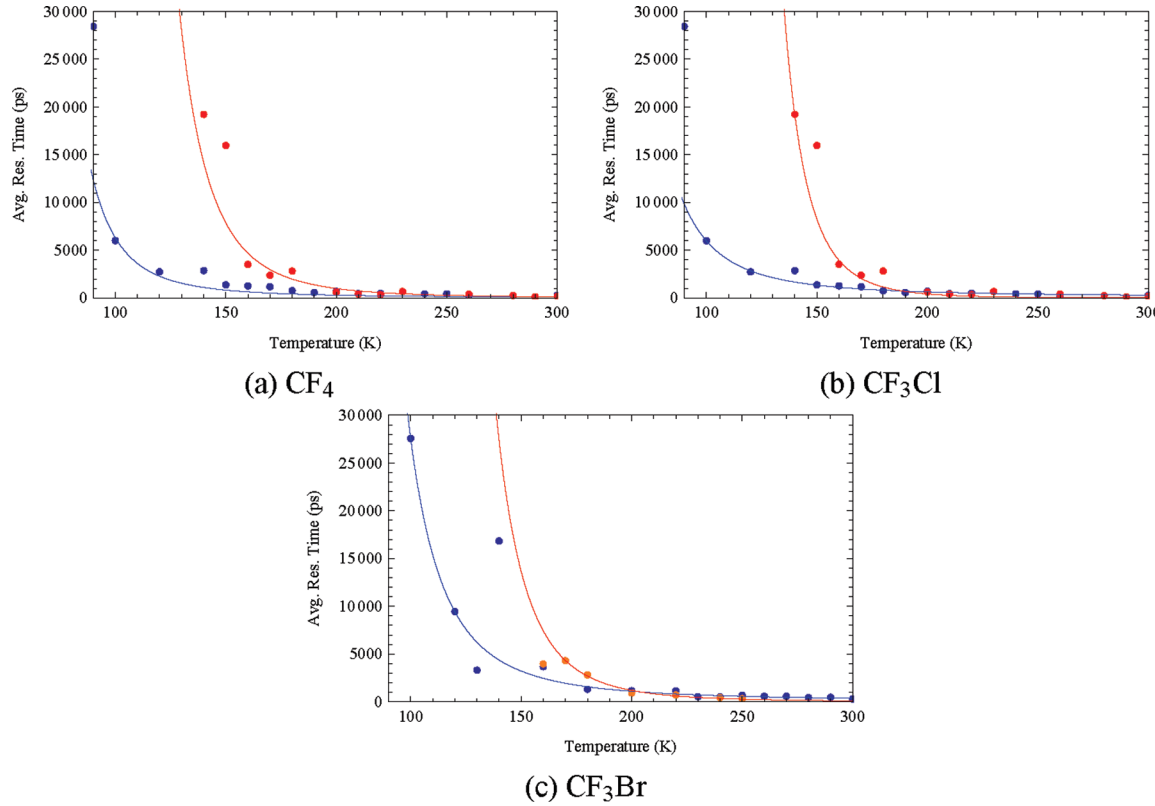

Figure 9. Average residence time as a function of temperature for first layers adsorbed on graphite (blue) and hydroxylated SiO_2 (red). Lines designate best-fit functions.

or near the surface of the substrate as well as the mean square displacement of molecules in the direction normal to the surface and parallel to the surface.

To calculate the average amount of time spent by a molecule in the first layer, we constructed a layer population function for molecules within a given layer in analogy with a prescription for the residence time of water molecules in the first coordination shell of a given solute ion by Impey et al.[35] In our case, the function is defined as

$$n_{\mathrm{mol}}(t) = \frac{1}{N_{\mathrm{tot}}} \sum_{i=1}^{N_{\mathrm{tot}}} \theta(t_0)\, \theta(t_0 + t) \qquad (6)$$

The sum runs over all molecules that are within the given layer at time t_0, and $\theta(t)$ is a unit step function whose value is 1 if the molecule is in the layer at time t and 0 otherwise (thus, $n_{\mathrm{mol}}(0) = 1$). Special care is given to discern molecules that left the layer and returned within a time Δt as not having entered the bulk; in this case, Δt was set at 2 ps. This gives us the fraction of molecules originally in the layer at time t_0 that have not escaped to the bulk after a time t. After the system was determined to have reached an equilibrium state, we calculated an average population function by averaging n_{mol} over a large interval of time to determine the average population of the equilibrium layer as a function of time.

The originally defined residence function from Impey et al., was found to be structured such that the behavior of the function with respect to time showed simple exponential decay, with $n_{\mathrm{mol}}(t) \sim n_{\mathrm{mol}}(0) \exp(-t/\tau)$, with characteristic time constant τ. In our case, the same general behavior is noted, with the caveat that the exponential decay should be moderated by a stretching parameter, so that our exponential decay became a stretched exponential (Kohlrausch−Williams−Watts, or KWW) decay, $n_{\mathrm{mol}}(t) \sim n_{\mathrm{mol}}(0) \exp[-(t/\tau_0)^{\beta}]$, where τ_0 is the characteristic decay time, and β is the stretching parameter. From the fitting of the data to the KWW function, we obtain the characteristic decay time, which can then be used to calculate the average decay time,

$$\langle \tau \rangle = \frac{\tau_0}{\beta} \Gamma\left(\frac{1}{\beta}\right)$$

which in turn gives us a convenient value for the comparative residence time of molecules in a given layer.

In Figure 9, we have calculated the mean residence time for the first adsorbed layer in each case and plotted the results as a function of system temperature. In each case, it is clear that the residence times for films adsorbed on the hydroxylated SiO_2 substrate demonstrate a significantly larger residence time at lower temperatures than the same films on the graphite substrate. It should be noted that in the case of films on hydroxylated SiO_2, some of the statistically significant data points existed outside the range of the simulation and were regarded as having nearly infinite residence time, owing to the premise that a large calculated residence time was a result of few, if any, molecules leaving the first layer within the time of the simulation.

At low temperatures, residence time calculations for films on either substrate show a great deal of temperature dependence, with small increases in temperature producing notable decreases in average residence time. If one continues to raise the temperature, however, these residence times approach similar values, which suggest that with sufficient increases in temperature, molecules are able enough to overcome barriers to desorption that the distinction between surface effects becomes less noticeable. Films adsorbed on graphite actually show a

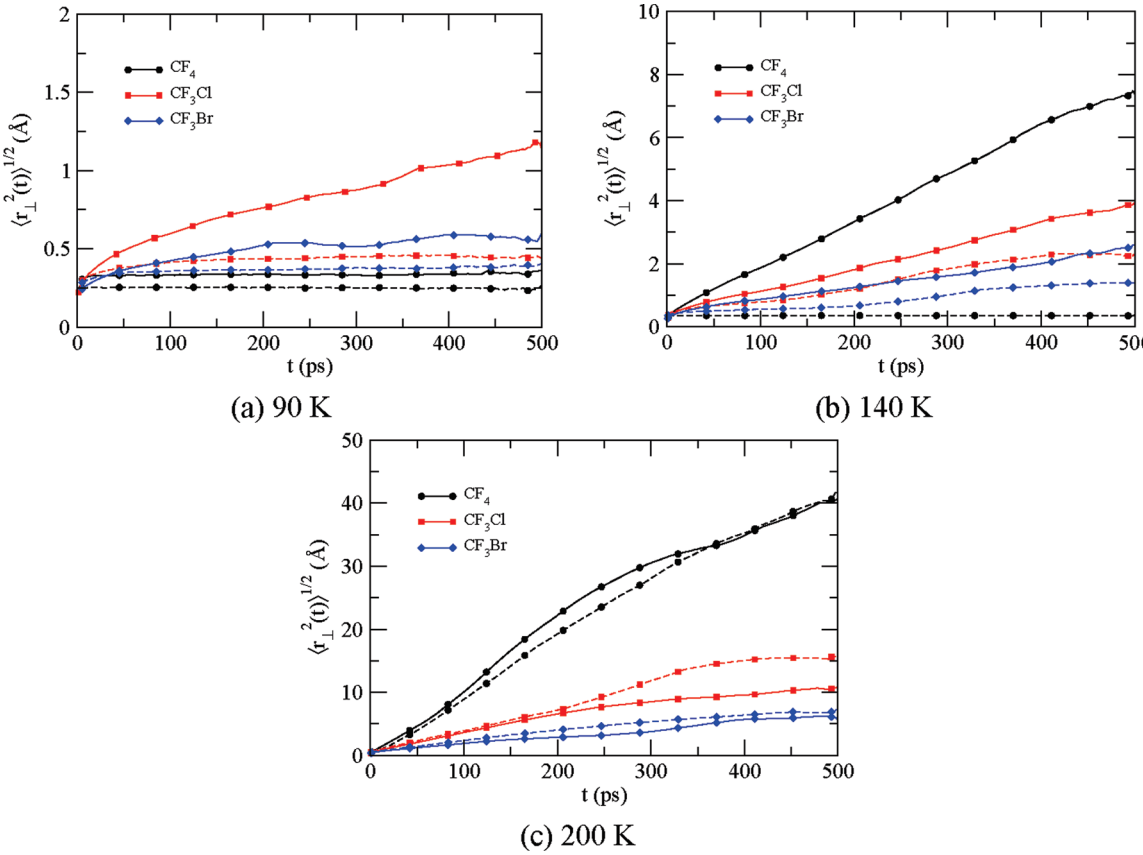

Figure 10. Component of root-mean-square displacement normal to surface at 90, 140, and 200 K as a function of time. Solid lines represent adsorption on graphite substrate; dashed lines represent adsorption on SiO_2.

much earlier transition to low residence times, which is in line with previous statements regarding the loss of structural order seen previously and the possibility of an implied melting transition.

Furthermore, it has been suggested[36] that a relationship exists between the energy of desorption of adatoms on a crystal surface and the residence time of the adatom. The relation bears the form of a simple exponential decay, $\tau = \tau_0 \exp(-E_d/k_B T)$, where E_d is the activation energy of desorption for a given temperature, T. If we assume such a decay, we can qualitatively assert a categorically higher activation energy of desorption for films adsorbed on hydroxylated SiO_2. This result correlates nicely with the resistance to lateral rearrangement seen in the structural analysis.

Mean Squared Displacement. A question remains, however, in why we see appreciable first-layer residence times for the polar molecules on the graphite substrate but detect little or no positional order when we examine the in-plane radial distribution function for the same cases. A possible explanation comes directly from the definitions given for these two quantities - first-layer residence time examines the tendency of molecules to stay in the layer closest to the substrate and not move toward the bulk adsorbate but says nothing about the positions of the molecules in the layer, while the in-plane radial distribution is designed to give a quantitative measure of exactly this, but only in relation to one another. To supplement these measures, we also examined the mean square displacement (MSD) of the molecules, focusing separately on the component of the MSD normal to the surface and the component parallel to the surface. Information from the MSD normal to the surface should offer insight into desorption from the surface that the first-layer residence time could not, such as how far molecules move toward the bulk adsorbate upon desorbing from the surface, while the component of MSD parallel to the surface should do the same for the in-plane radial distribution function, showing not just whether molecules coalesce into a specific arrangement but offering clues as to how far and how fast the average molecule laterally displaces itself as a function of time.

We observed the MSD for each case for 0.5 ns after the system had reached equilibrium to look at the basic motion of the molecules. In Figure 10, we observe the component of the root-mean-square displacement normal to the surface for three representative temperatures −90 K, below or near the bulk melting temperatures of the adsorbates (very slightly above, in the case of CF_4); 140 K, above the bulk melting temperatures of all three adsorbates but still below their atmospheric-pressure boiling points; and 200 K, above the boiling points of all three adsorbates. In Figure 10a, we see that the low-temperature cases behave as might be expected of a crystalline or crystalline-like first layer; each adsorbate shows very little motion into the bulk: less than 1.25 Å in all cases, and ∼0.5 Å or less in all but one. From the mass density (Figure 1), the spacing between layers is shown to be on the order of 3−4 Å and thus in these cases molecules are highly unlikely to leave the first layer.

In Figure 10b, at 140 K, we see increased mobility for each adsorbate type, with pronounced increases in motion away from the surface for molecules adsorbed on graphite; this is in line with our residence time calculations, which suggest molecules are less likely to remain on the first layer at this temperature, even more so on the graphite substrate versus the SiO_2 substrate. CF_4 on SiO_2 is something of an anomaly here, as the normal MSD suggests CF_4 molecules are only slightly more mobile at 140 K than they were at 90 K; this result, however, is borne out by examination of the in-plane radial distribution function

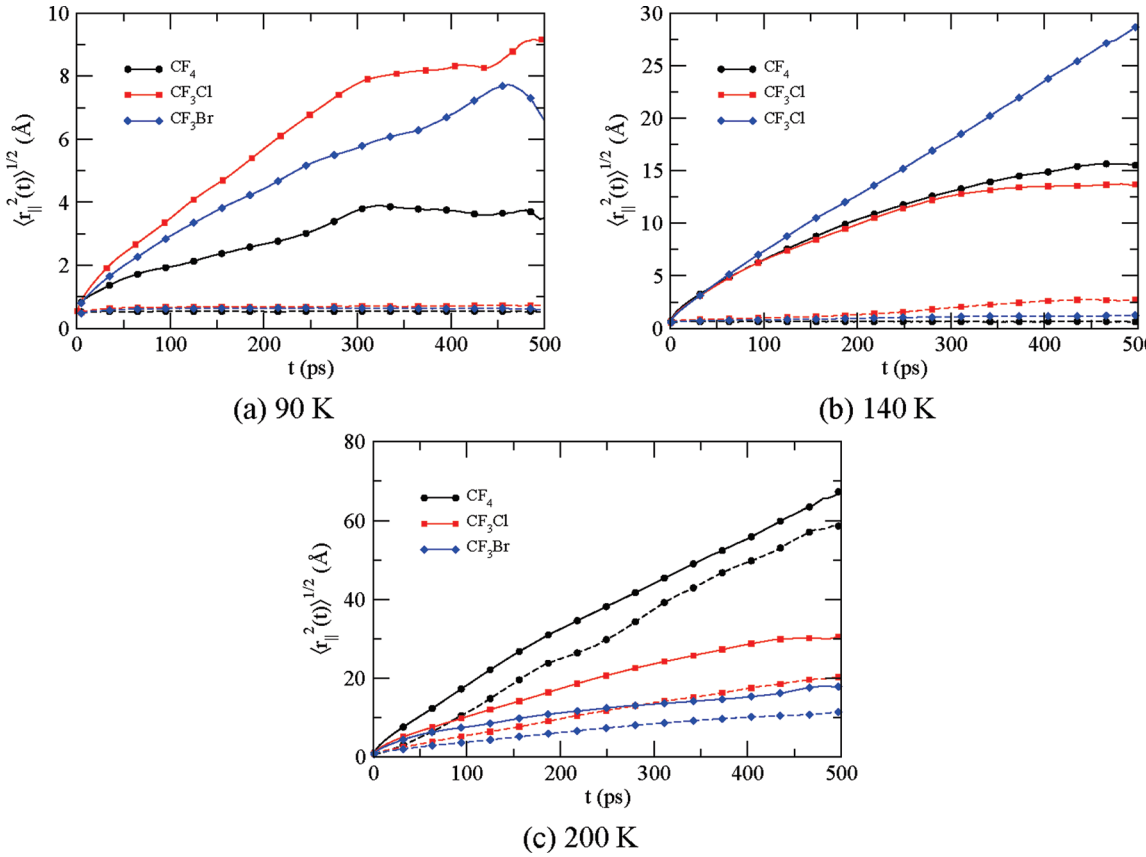

Figure 11. Component of root-mean-square displacement parallel to the surface at 90, 140, and 200 K as a function of time. Solid lines represent adsorption on graphite substrate; dashed lines represent adsorption on SiO_2.

(Figure 5) and the 6-fold order parameter Ψ_6, which suggests that this surface is quite able to maintain a high degree of order well above the bulk melting temperature. In Figure 10c, we see the effect of further increasing the temperature, as in each case here, the distinction between the mobility of first-layer molecules on graphite versus SiO_2 is largely absent; the conclusion here is that at sufficient temperatures, thermal energy imparted to the molecules as kinetic energy is able to overcome the barrier to desorption, and molecules become largely free to move into the bulk adsorbate. This description matches well with the decreased residence time for first-layer molecules, as well as the decreases in positional order from the in-plane radial distribution function and 6-fold order parameter. Combined with what we know about the density, this would serve to reinforce the observation of a phase transition. Specific study of this transition in a further exercise may be able to elucidate the precise meaning of the increase in mean square displacement.

In Figure 11, referencing the motion of molecules along the surface, the difference between adsorption on graphite versus SiO_2 is even more pronounced. At 90 K, near the low end of our simulation range and below the bulk melting temperatures of both polar cases, we see a dramatically higher in-plane MSD for molecules adsorbed on graphite than for those adsorbed on SiO_2. Indeed, for these cases, while the lateral mobility of CF_4 on graphite is only on the order of one molecule diameter, the polar cases show that the average molecule is moving 2−3 molecular diameters in just 0.5 ns. This helps explain the relatively quick relaxation seen in the in-plane radial distribution function for CF_4 on graphite, as well as the nearly complete lack of positional order seen in the polar films adsorbed on graphite; apparently, attraction to the graphite substrate is able to provide a sufficient barrier to desorption at low temperatures, but it does very little to limit the lateral movement of molecules along the surface. This suggests while the CF_4 film on graphite may be classified as crystalline at low temperatures, the films of the polar molecules on graphite are harder to categorize; the degree of movement seen suggests a more fluid layer, but the fact that the normal-direction MSD still shows a resistance to desorption suggests that may not be precisely in the liquid phase, which is likely the source of the ambiguous structure seen in the in-plane radial distribution function.

On the other hand, all three films on SiO_2 show a high degree of restriction of movement, less than 0.5 Å in all cases. Previous visualizations (Figure 7) further support the conclusion that the hexagonal arrangement of hydroxyl groups at the surface creates a network of "cells" that envelop the adsorbed molecules, allowing minor displacements from the centers of the hexagons, but not allowing molecules to closely approach or cross over the hydroxyl groups. Further, at low temperatures, this effect appears to have roughly the same strength regardless of whether the adsorbate molecules are polar or nonpolar.

The effect also remains at higher temperatures. As suggested by the 6-fold order parameter as well as the in-plane radial distribution function, the apparent confinement effect of the hydroxylated SiO_2 surface remains at 140 K, and likely higher. In this case, small separation can be seen between the CF_4 film on SiO_2 and the polar molecules, and in general, the in-plane MSD suggests slightly higher mobility for the polar molecules (although still at the level of ∼2 Å or less), but the difference between the mobility of the molecules on this substrate versus the same molecules on the graphite substrate is profound. On graphite, the in-plane MSD shows displacements of between 12 Å (CF_3Cl, CF_4) and nearly 30 Å (CF_3Br), more than an order of magnitude difference compared to adsorption on SiO_2. As

expected, though, there is a limit to this confinement effect; at higher temperatures sufficient to impart more kinetic energy on the molecules, the differences in in-plane MSD dwindle or disappear, and molecules show similar mobilities regardless of substrate type. It is also worth noting that at higher temperatures, where the substrate-type effect is less pronounced or completely overcome, there appears a relationship between the MSD, both parallel to the surface and normal to it, and the mass of the adsorbate molecule (larger average displacements for lighter molecules) that may be expected in these situations, when the molecules are not as encumbered by interactions with the surface.

Conclusions

In this study, we have attempted to elucidate the adsorption behavior of one polar compound (CF_4) and two related polar compounds (CF_3Cl and CF_3Br) on two atomically flat but chemically different substrates (graphite and hydroxylated SiO_2). We had expected that the phobicity of the substrates (hydrophobic graphite vs hydrophilic SiO_2) as well as the difference in polar nature of the adsorbate molecules would play important roles in determining both the structure and dynamics of surface layers, and evidence obtained from analysis of both points to significant effects arising from the differences studied. Interactions between hydroxyl groups on the surface of our hydroxylated SiO_2, creating a hexagonal network of hydrogen-bonded hydroxyls, served as the main impetus for both dramatic changes in structure and packing arrangements as well as dynamic considerations such as mean squared displacement and adsorbate molecule residence time.

As in a previous result,[27] the result of simulations of all three adsorbate molecules may be thought of as being a function of the available adsorption sites. Previous studies[4] have suggested that the graphite surface allows for three different types of adsorption site—directly over the bond joining adjacent carbon atoms (bridge), directly above a carbon atom (atop), or precisely in the center of a graphite hexagon (center)—and prefers two of these sites (bridge and atop) creating a number of equivalent or nearly equivalent adsorption sites. Conversely, in our simulations, we have observed that the propensity of hydroxyl groups on the surface of hydroxylated SiO_2, and the apparent associated barrier with adsorption near the hydrogen bond network, prevent many analogous sites on hydroxylated SiO_2 from being usable and leaves only center sites as preferred adsorption sites on this substrate.

This pivotal difference in the hydroxylated SiO_2 surface has profound effects on the adsorption behavior of all three species studied. Perhaps because molecules adsorbed on graphite have a number of adsorption sites to choose from, and a lower energy barrier to desorption, the structure of layers seen on graphite substrates are much more susceptible to variations in temperature, causing only a modest extension of the expected phase boundaries of the bulk adsorbates and much less definition in packing arrangements. Molecules adsorbed on graphite are thus observed to show limited positional and translational order, do not hold this order well when thermal energy is added to the system, and are shown to desorb with quickly increasing frequency as a function of increased temperature.

Films adsorbed on hydroxylated SiO_2, however, are bound by interactions with the hydrogen bonding network on the surface of the substrate. These interactions serve to very efficiently limit the translational freedom of adsorbed species, forcing adsorbed molecules into highly ordered packing arrangements that withstand much greater increases in temperature and providing a greater barrier to desorption that is generally overcome only at temperatures above what is expected to cause a transition to the vapor phase.

Acknowledgment. We gratefully acknowledge the Donors of the American Chemical Society Petroleum Research Fund Grant No. PRF# 47785-G6 and NSF Grant No. DMR0847580 for support of this research. We also thank Dr. Chris D. Lorenz (King's College London) and Chriranjivi Lamsal (Southern Illinois University, Carbondale) for helpful conversations.

References and Notes

(1) Kirsch, P. *Modern Fluoroorganic Chemistry: Synthesis, Reactivity, Applications*; Wiley-VCH: Weinheim, Germany, 2004.
(2) O'Hagan, D. *Chem. Soc. Rev.* **2008**, *37*, 308–319.
(3) Kjaer, K.; Nielsen, M.; Bohr, J.; Lauter, H. J.; McTague, J. P. *Phys. Rev. B* **1982**, *26*, 5168–5174.
(4) Pinches, M. R. S.; Tildesley, D. J. *Surf. Sci.* **1996**, *367*, 177–195.
(5) Zhang, Q. M.; Kim, H. K.; Chan, M. H. W. *Phys. Rev. B* **1986**, *34*, 2056–2059.
(6) Zhang, Q. M.; Kim, H. K.; Chan, M. H. W. *Phys. Rev. B* **1986**, *34*, 8050–8063.
(7) Nham, H. S.; Drir, M.; Hess, G. B. *Phys. Rev. B* **1987**, *35*, 3675–3678.
(8) Bruch, L. W. *J. Chem. Phys.* **1987**, *87*, 5518–5527.
(9) Heroux, L.; Krungleviciute, V.; Calbi, M. M.; Migone, A. D. *J. Phys. Chem. B* **2006**, *110*, 12597–12602.
(10) Yaws, C. L. *Thermophysical Properties of Chemicals and Hydrocarbons*; William Andrew/Elsevier: Norwich, NY, U.S., 2008.
(11) Connolly, M. J.; Roth, M. W.; Gray, P. A.; Wexler, C. *Langmuir* **2008**, *24*, 3228–3234.
(12) Gus'kova, O. A.; Mena-Osteritz, E.; Schillinger, E.; Khalatur, P. G.; Bäuerle, P.; Khokhlov, A. R. *J. Phys. Chem. C* **2007**, *111*, 7165–7174.
(13) Maolin, S.; Fuchun, Z.; Guozhong, W.; Haiping, F.; Chunlei, W.; Shimou, C.; Yi, Z.; Jun, H. *J. Chem. Phys.* **2008**, *128*, 134504.
(14) Tsige, M.; Soddemann, T.; Rempe, S. B.; Grest, G. S.; Kress, J. D.; Robbins, M. O.; Sides, S. W.; Stevens, M. J.; Webb, E. *J. Chem. Phys.* **2003**, *118*, 5132–5142.
(15) Tsige, M.; Patnaik, S. S. *Chem. Phys. Lett.* **2008**, *457*, 357–361.
(16) Watkins, E. K.; Jorgensen, W. L. *J. Phys. Chem.* **2001**, *105*, 4118–4125.
(17) Jorgensen, W. L.; Maxwell, D. S.; Tirado-Rives, J. *J. Am. Chem. Soc.* **1996**, *118*, 11225–11236.
(18) Plimpton, S. J. *J. Comput. Phys.* **1995**, *117*, 1–19, may be found at lammps.sandia.gov.
(19) Hockney, R. W.; Eastwood, J. W. *Computer Simulation Using Particles*; Taylor & Francis Group: New York, NY, U.S., 1988.
(20) Kudchadker, A. P.; Kudchadker, S. A.; Patnaik, P. R.; Mishra, P. P. *J. Phys. Chem. Ref. Data* **1978**, *7*, 425–439.
(21) Xiang, H. W. *J. Phys. Chem. Ref. Data* **2002**, *30*, 1161–1197.
(22) Weimer, W.; Knorr, K.; Wiechert, H. *Phys. Rev. Lett.* **1988**, *61*, 1623–1626.
(23) Sakata, M.; Cowlam, N.; Davies, H. A. *J. Phys. F: Met. Phys.* **1979**, *9*, 235–240.
(24) Szczygielska, A.; Burian, A.; Duber, S.; Dore, J. C.; Honkimaki, V. *J. Alloys Compd.* **2001**, *328*, 231–236.
(25) Knorr, K.; Fassbender, S.; Warken, A.; Arndt, D. *J. Low Temp. Phys.* **1998**, *111*, 339–348.
(26) Pawley, G. S.; Hewat, A. W. *Acta Crystallogr.* **1985**, *B41*, 136–139.
(27) Leuty, G.; Nehring, J.; Tsige, M. *Surf. Sci.* **2009**, *603*, 3374–3381.
(28) Fassbender, S.; Enderle, M.; Knorr, K.; Noh, J. D.; Rieger, H. *Phys. Rev. B* **2002**, *65*, 165411.
(29) Humphrey, W.; Dalke, A.; Schulten, K. *J. Mol. Graph.* **1996**, *14*, 33–38.
(30) Yang, J.; Wang, E. G. *Phys. Rev. B* **2006**, *73*, 035406.
(31) Miranda, J. M. G.; Torra, V. *J. Phys. F: Met. Phys.* **1983**, *13*, 281–289.
(32) Yoon, B. J.; Jhon, M. S.; Eyring, H. *Proc. Natl. Acad. Sci. U. S. A.* **1981**, *78*, 6588–6591.
(33) Marzec, M.; Kuchta, B.; Firlej, L. *J. Mol. Model.* **2007**, *13*, 537–542.
(34) Hung, F. R.; Coasne, B.; Santiso, E. E.; Gubbins, K. E.; Siperstein, F. R.; Sliwinska-Bartkowiak, M. *J. Chem. Phys.* **2005**, *122*, 144706.
(35) Impey, R. W.; Madden, P. A.; McDonald, I. R. *J. Phys. Chem.* **1983**, *87*, 5071–5083.
(36) Gladyszewski, L. *Vacuum* **1995**, *46*, 407–409.

JP1065049